Hindawi Publishing Corporation
Journal of Nanomaterials
Volume 2015, Article ID 240948, 8 pages
http://dx.doi.org/10.1155/2015/240948

Research Article

Effect of the Surfactant on the Growth and Oxidation of Iron Nanoparticles

Alvaro Ruíz-Baltazar,[1] Rodrigo Esparza,[1] Gerardo Rosas,[2] and Ramiro Pérez[1]

[1]*Center for Applied Physics and Advanced Technology, National Autonomous University of Mexico, Boulevard Juriquilla 3001, 76230 Santiago de Querétaro, QRO, Mexico*
[2]*Metallurgical Research Institute, Michoacan University of Saint Nicholas of Hidalgo, Building U, University City, 58000 Morelia, MICH, Mexico*

Correspondence should be addressed to Alvaro Ruíz-Baltazar; alvarodejesusruiz@yahoo.com.mx

Received 1 May 2015; Revised 6 June 2015; Accepted 21 June 2015

Academic Editor: Nguyen D. Hoa

Fe nanoparticles and branched nanostructures of iron oxide were synthesized by chemical reduction in aqueous phase. The mechanism of formation of iron oxides as a function of the amount of surfactant employed during the synthesis process was studied. Specifically Fe, Fe_2O_3, and Fe_3O_4 nanoparticles were obtained. The oxidation of Fe to Fe_3O_4 and finally to Fe_2O_3 was carried out by oxidative etching process, decreasing the amount of stabilizer agent. The structures obtained were characterized by high resolution (HRTEM) and scanning/transmission (STEM) electron microcopies, energy dispersive spectroscopy (EDS), and optical spectroscopy (UV-Vis and IR).

1. Introduction

In recent years iron oxide nanoparticles have been extensively studied, due to their wide applications in biomedical treatments, magnetic fluids, groundwater remediation, hazardous waste treatment, catalytic degradation, microwave adsorption, medical diagnostic, and magnetic recording [1–5]. These studies have also been induced by their superparamagnetic and catalytic properties [6, 7]. Several synthesis routes to obtain Fe_3O_4 magnetic nanoparticles have been reported including the chemical reduction, coprecipitation, hydrothermal process, and polyol and sol-gel methods [8–11]. However, the chemical reduction method offers an effective route to obtain very well-defined homogeneous nanoparticles sizes and morphologies. For technological applications, it is important to develop nanoparticle dispersions without aggregation or coalescence [12]. During colloidal synthesis, the nanoparticles need to be passivized to prevent coalescence. A lesser amount of surfactant than the optimum, where the surfactant does not perfectly cover the entire surface of the particles, can cause coalescence of the particles or uncontrolled increasing in particle size [13]. Specifically, in this study, Fe, Fe_2O_3, and Fe_3O_4 nanoparticles were synthesized by chemical reduction. Fe(III) chloride hexahydrate ($FeCl_3{\cdot}6H_2O$) was employed as starting metallic salt and polyvinyl pyrrolidone (PVP) as surfactant agent. As well documented in the literature, stabilizer agent determines the size and shape of the iron nanostructures [6, 14]. The oxidation degree and morphology obtained in this process are described and discussed in terms of the amount of the stabilizing agent present in the reaction.

2. Materials and Methods

The synthesis of iron nanostructures was carried out by the chloride method modified [15]. In this case, $FeCl_3{\cdot}6H_2O$ as precursor and polyvinyl pyrrolidone (PVP) as surfactant were used. For the reduction of the metallic salt, sodium borohydride ($NaBH_4$) was employed. All reagents were provided by Sigma Aldrich with a purity of 99.98%. Three samples of nanoparticles were synthesized by the same synthesis route. In the first two samples (S1 and S2), equal concentrations of ferric chloride (0.01 M) were used, while in the third sample (S3) a concentration of 0.08 M was used.

Table 1: Amounts of reagents used in the synthesis process.

Sample	Concentration [M]			Ratio	
	$FeCl_3{\cdot}6H_2O$	PVP	$NaBH_4$	$FeCl_3{\cdot}6H_2O/NaBH_4$	$PVP/FeCl_3{\cdot}6H_2O$
S1	0.01	1	0.02	0.5	100
S2	0.01	0.5	0.02	0.5	50
S3	0.08	0.1	0.02	4	1.25

The variable parameter in the process of synthesis was the concentration of stabilizing agent, for which concentrations of 1.0, 0.5, and 0.1 M were added to S1, S2, and S3 samples, respectively. The reaction was carried out at room temperature and a constant pH of the colloidal medium of 11. Table 1 specifies the synthesis conditions employed by the produced Fe nanostructures.

This method is based on the Fe^{3+} ions reduction using sodium borohydride ($NaBH_4$) as reducing agent according to the following reaction [15]:

$$4Fe_{(aq)}{}^{3+} + 3BH_{4(aq)}{}^{-} + 9H_2O \longrightarrow 4Fe_{(s)}{}^{0} + 3H_2BO_{3(aq)}{}^{-} + 12H_{(aq)}{}^{-} + 6H_{2(g)} \quad (1)$$

In general form, this reaction is conducted in two phases, initially by the ($NaBH_4$) decomposition generating hydrogen. Subsequently, hydrogen is responsible for the reduction of Fe^{3+} to Fe^0 [15].

The structural and morphological characteristics of the dispersed metallic nanoparticles have been studied using a Philips Tecnai F20 transmission electron microscope (TEM) with a field emission gun attachment and dot to dot direct maximum resolution of 0.23 nm. TEM specimens were prepared by dispersing and subsequent drying of a drop of colloidal solution on a copper grid (3 mm in diameter) covered with an amorphous carbon film. Energy dispersive (EDS), X-ray diffraction (XRD), ultraviolet visible (UV-Vis), and infrared (IR) studies were also conducted.

3. Results and Discussion

3.1. Transmission Electron Microscopy. Transmission electron microscopy (TEM) was used to observe the size and morphology of the nanoparticles. Figure 1(a) shows a bright field TEM image at low magnification from the Fe nanoparticles stabilized with 1.0 M PVP (sample S1). The morphology of the nanoparticles is spherical and the formation of agglomerates is not appreciated. This result can be attributed to the higher amount of stabilizing agent used in this sample and consequently a less interaction between the Fe surface area and the colloidal medium. The large amount of PVP used prevented the agglomeration and the oxidation of the particles. Figure 1(b) shows the chemical analysis by energy dispersive spectroscopy (EDS) from the sample S1. As can be observed in the spectrum, only the Fe signal was obtained (the C and Cu are located in the grid). Figure 1(c) shows a single Fe nanoparticle, the average particle size is 12 nm, and nonjoined particles are appreciable. To analyze the structure of the Fe nanoparticle, HREM images were performed. Figure 1(d) shows a small region of the single Fe nanoparticle where d-spacings of 0.2128, 0.2085, and 0.1858 nm were obtained. These d-spacings correspond to the $(1\bar{1}1)$, $(\bar{1}\bar{1}1)$, and (200) planes, respectively (Figure 1(e)), of the fcc structure of the Fe (65-4150).

Decreasing the amount of PVP by 50 percent during second synthesis (sample S2), the oxidation of Fe nanoparticles is induced. It should be noted that oxidation of Fe nanoparticles is evident, due to the interaction with the environment generating Fe_3O_4 particles. Figure 2(a) shows a transmission electron microscopy (TEM) image at low magnifications, where the distribution and size of Fe_3O_4 magnetic nanoparticles are observed. The effective diameter of the particles is about 50 nm. Figure 2(b) shows a filtered HRTEM image corresponding to Fe_3O_4 nanoparticle. The main interplanar distance measured was 0.485 nm corresponding to the planes (220) of magnetite Fe_3O_4 (19-0629). Finally, Figure 2(c) describes the power spectrum (FFT) of magnetite Fe_3O_4. The FFT shows the characteristic interplanar distances of the magnetite Fe_3O_4. Note that this result is consistent with the synthesis conditions presented in the experimental methodology; evidently the action of the surface active agent is diminished considerably, resulting in growing due to the oxidation of the iron nanoparticles.

Figures 3(a)–3(c) show bright field TEM images of Fe_2O_3 nanostructures (sample S3), which have a morphology of branched nanostructures approximate of 200 nm in size. This is due to the decreased amount of PVP in the aqueous solution, generating a greater oxidation and consequently a growth of Fe_2O_3 structures. On the other hand, some studies indicate that the formation of Fe_2O_3 nanostructures is due to the oxidation of magnetite (Fe_3O_4) colloidal solutions and the decrease in the amount of surface active agent used in the process of synthesis [16]. Also, it has been reported in the literature that the oxidation process is carried out primarily on the corners and edges of the nanocrystals giving rise to high reactivity regions. However, an isotropic growing takes place over the entire surface of nanocrystals where the more active sites have been oxidized. Indeed this situation depends on the surface chemical nanocrystals [6, 16, 17]. HRTEM image of a tip of the Fe_2O_3 nanostructures is presented in Figure 3(d), identifying a distance between planes of 0.601 nm, which corresponds to the (110) plane of Fe_2O_3 structure (39-1346). STEM images (Figures 3(e)-3(f)) confirm the branched morphology of the Fe_2O_3 nanostructures with a uniform phase composition.

It is important to mention that, in addition to the use of ($NaBH_4$) as reducing agent, this synthesis route involves oxidative species such as oxygen, Fe(III) in solution,

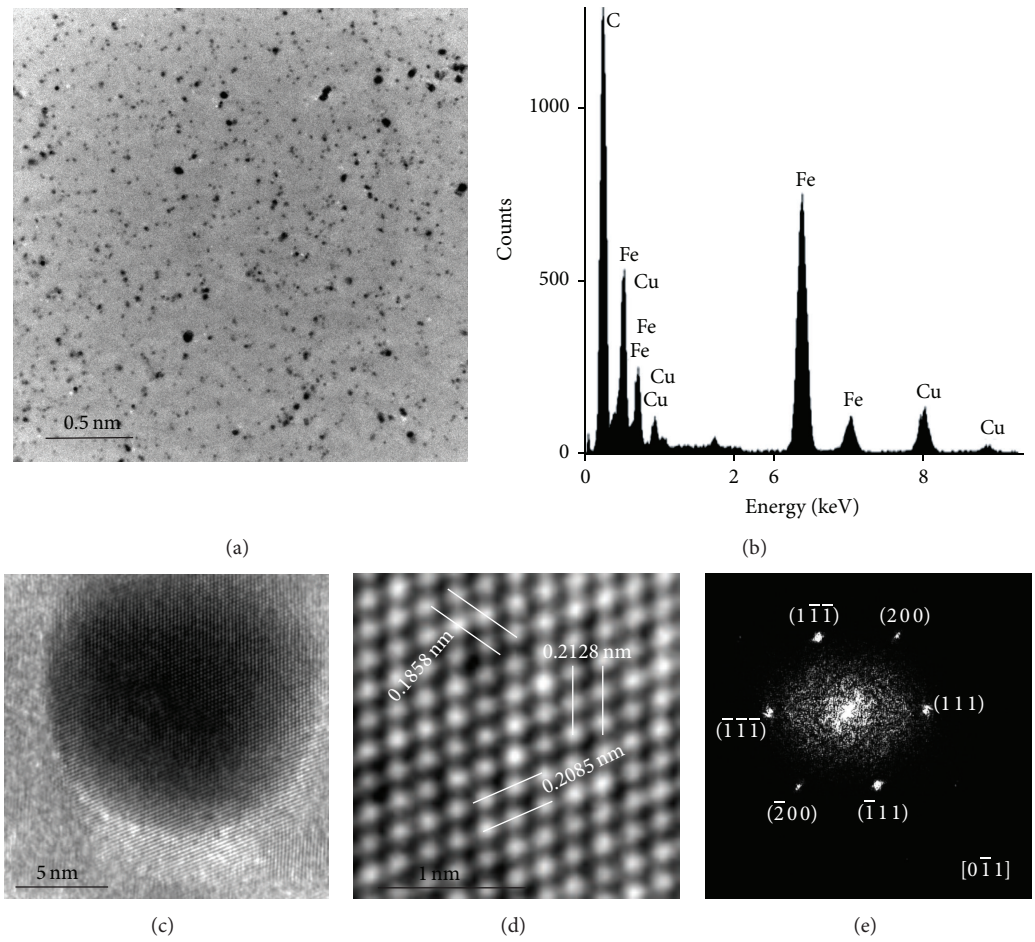

Figure 1: Fe nanoparticles: (a) image of low magnifications, (b) chemical EDS analysis from the sample of Fe, (c) HRTEM of single Fe, (d) small region of the single particle, and (e) FFT from axis zone [0$\bar{1}$1].

and corrosive ions as chlorides; this species promotes the oxidation process, specifically, the oxidative etching. This phenomenon is common in nature, which can be explained analogously to the corrosion of steel by air and/or water [6]. Accordingly it can be assumed that the synthetized iron particles experienced an oxidation of this nature. This is because, in this route of synthesis, the pH solution is constant and only the amount of PVP used in the synthesis process determines the formation of Fe nanostructures.

This is due to the fact that the surfactant agent modifies the iron nanoparticles surface and increases their active surface sites. Therefore, the PVP amount employed in the synthesis procedure is essential in the nucleation and growth process of Fe nanostructures. It can be deduced that the Fe particles obtained from the reduction of Fe^{+3} by $NaBH_4$ can be considered as growth cores of the iron oxides. In this sense, Fe particles were synthesized with the largest amount of PVP and therefore they were better stabilized. This fact indicates that Fe surface is less susceptible to oxidative etching.

However it is important to highlight and confirm the differences in the iron oxide phases (Fe_3O_4 and Fe_2O_3) corresponding to the S2 and S3 samples. Due to the fact that d-spacings corresponding to Fe_3O_4 and Fe_3O_2 are very similar, complementariness technique was conducted.

Table 2: Quantitative analysis of the elements Fe and O of samples S2 and S3.

Element	% Fe	% O	Fe/O	O/Fe
S2	76.72	23.28	3.295	0.303
S3	61.14	38.86	1.573	0.635

3.2. EDS Chemical Analysis. Figures 4(a) and 4(b) show the EDS spectrums of the S2 and S3 samples. In both cases the presence of Fe and O was observed. However, with the purpose of assessing the iron oxides phases of the samples, the atomic Fe/O ratio was obtained. This analysis was performed directly by the number of counts corresponding to the Fe and O peaks. Table 2 indicates the Fe and O quantification.

Based on the elemental analysis of the S2 and S3 samples, Fe/O ratio is in the order of 3.29 and 1.53, respectively. Similar values have been reported and were associated with the Fe_3O_4 and Fe_2O_3 [18, 19]. This result highlights the presence of both iron oxide phases observed by TEM.

Figures 5(a) and 5(b) show the X-ray diffraction pattern of the S2 and S3 samples, respectively. In this sense, both patterns are very similar. This fact is attributed to the magnetite and maghemite presents a cubic structure and

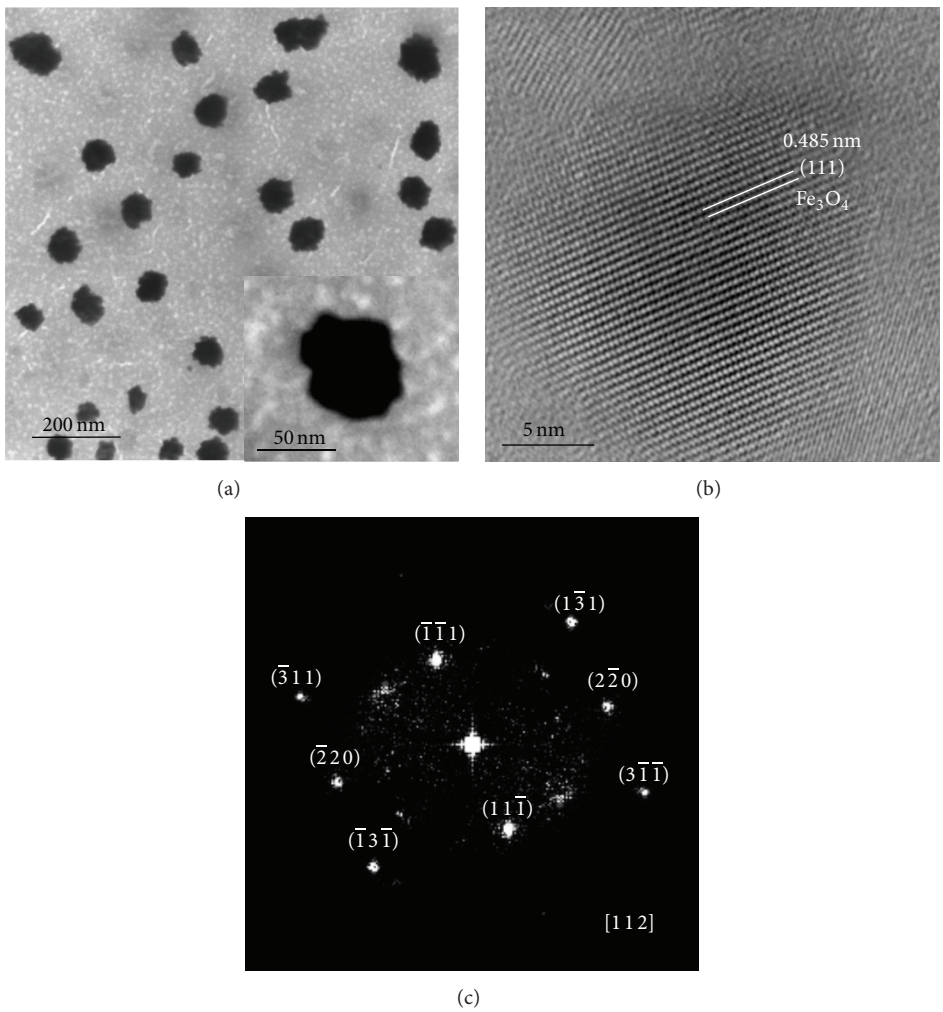

FIGURE 2: Fe_3O_4 nanoparticles: (a) TEM image at low magnification, (b) filtered HRTEM image of Fe_3O_4, and (c) FFT of the Fe_3O_4 particle.

lattice parameters are very close; for this reason, it is difficult to differentiate these structures even if both phases exhibit high crystallinity. However, some authors report that in the XRD pattern associated with the maghemite phase there exist two additional peaks located at 23.77° (210) and 26.10° (211). These intensities can be used to differentiate the magnetite phase [20–22].

In Figure 5(b) both intensities are clearly visible and therefore an oxidation is confirmed on the surface of the nanoparticles attributed to the decrease of the amount of stabilizing agent. XRD analysis supports and further confirms the presence of magnetite and maghemite, promoted by oxidative etching.

In order to evidence the absorption characteristics of the Fe, Fe_3O_4, and Fe_2O_3 structures, which were completely identified and verified by TEM, EDS, and XRD techniques, a spectroscopic study of samples is presented below.

3.3. UV-Vis and Infrared Spectroscopy. Figure 6(a) shows the UV-Vis spectra corresponding to the synthesized samples with different amounts of PVP (1.0, 0.5, and 0.1 M). It has been reported that in the nanoparticles of iron oxides almost no absorption is beyond 700 nm [18]. Some authors indicate that as the degree of oxidation increases in the Fe particles, the diffuse reflectance is greater [23]. For this reason it is clearly observed that synthesized samples with lesser amounts of PVP (0.01 M) have less absorbance; this is due to its high degree of oxidation particles. These results confirm the presence of nanoparticles Fe, Fe_3O_4, and Fe_2O_3 as a function of the amount of surfactant in each synthesis. Additionally it is observed that the Fe nanoparticles are better stabilized; therefore the degree of oxidation is not perceived and the absorbance is greater. In the case of Fe_3O_4 and Fe_2O_3 nanoparticles the oxidation process is evident, due to the formation of maghemite (Fe_2O_3) as a result of oxidation of the magnetite (Fe_3O_4) [6, 24]. The decrease in the amount of PVP promoted the oxidation process of Fe nanoparticles and consequently an increase in the particle size of iron oxides nanoparticles. This result confirms the morphologies and particle sizes observed by transmission electron microscopy. Therefore, it is observed that the particles with a greater degree of oxidation have a greater particle size. This fact is attributed to the oxidation process that is carried out on the surface of the nanoparticles. In this sense, the particles with

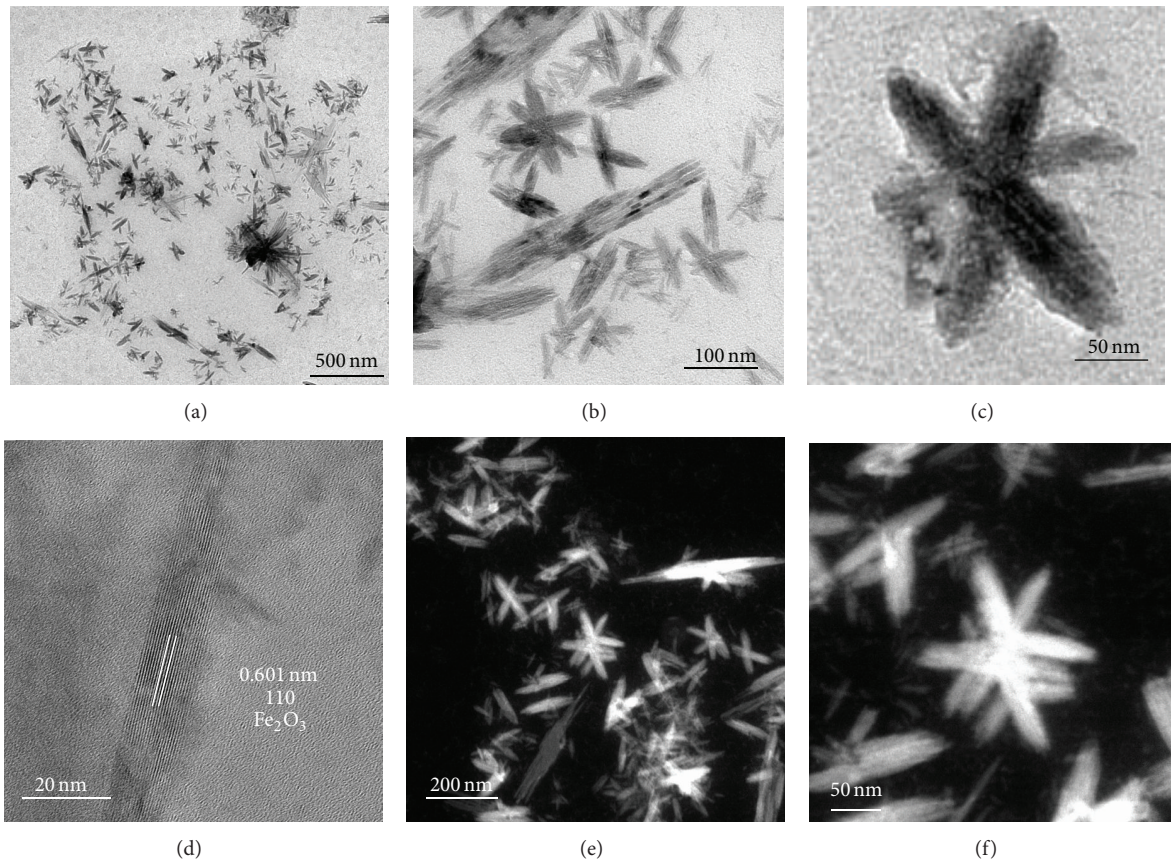

FIGURE 3: (a), (b), and (c) Bright field TEM images of Fe_2O_3 structures, (d) HRTEM image with interplanar distance associated with the (110) plane of Fe_2O_3, and (e) and (f) STEM images corresponding to Fe_2O_3 nanostructures.

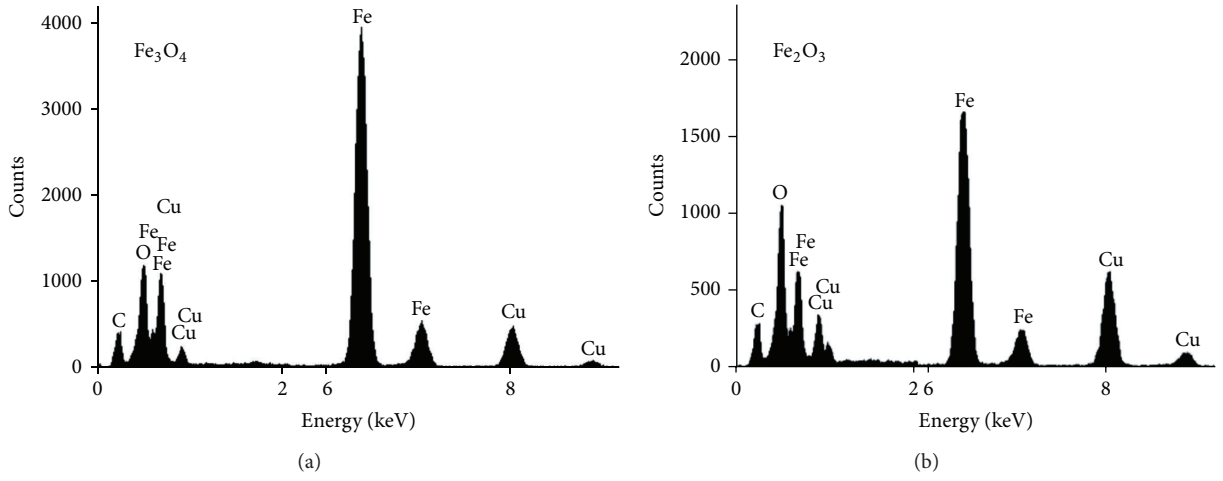

FIGURE 4: EDS spectrum of (a) sample S2 (Fe_3O_4) and (b) sample S3 (Fe_3O_4).

larger sizes promote the sedimentation of the samples that are in aqueous solution. Therefore the absorbance of these particles is reduced.

Figure 6(b) shows the IR-spectrum of the nanoparticles of the S1, S2, and S3 samples. In the sample S1 (Fe nanoparticles), Fe-O bonds are not observed. In the S2 and S3 samples, two main absorption bands are observed. The band located at 668 cm^{-1} is associated with stretching vibration existing between Fe-O bonds [18–21]. The band located at 1633 cm^{-1} is assigned to O-H vibrations absorbed on the surface of Fe nanostructures [20, 21]. S2 shows a specific intensity at 684 cm^{-1}, which confirms the presence of magnetite [25]. A characteristic absorption peak located at 793 cm^{-1} can be attributed to the maghemite structure [26]. However, in the

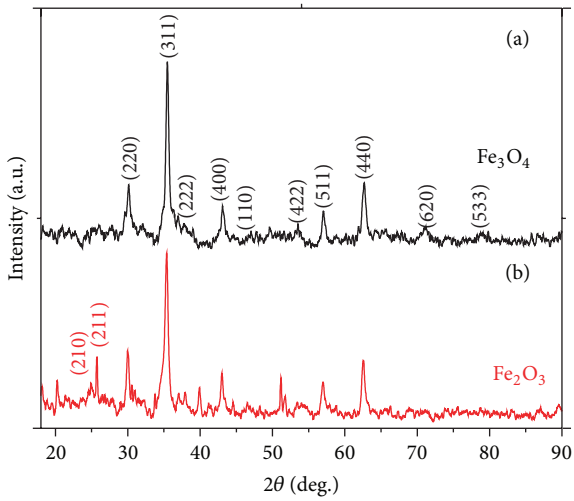

FIGURE 5: XRD pattern of the (a) magnetite Fe_3O_4 and (b) maghemite Fe_2O_3 structures.

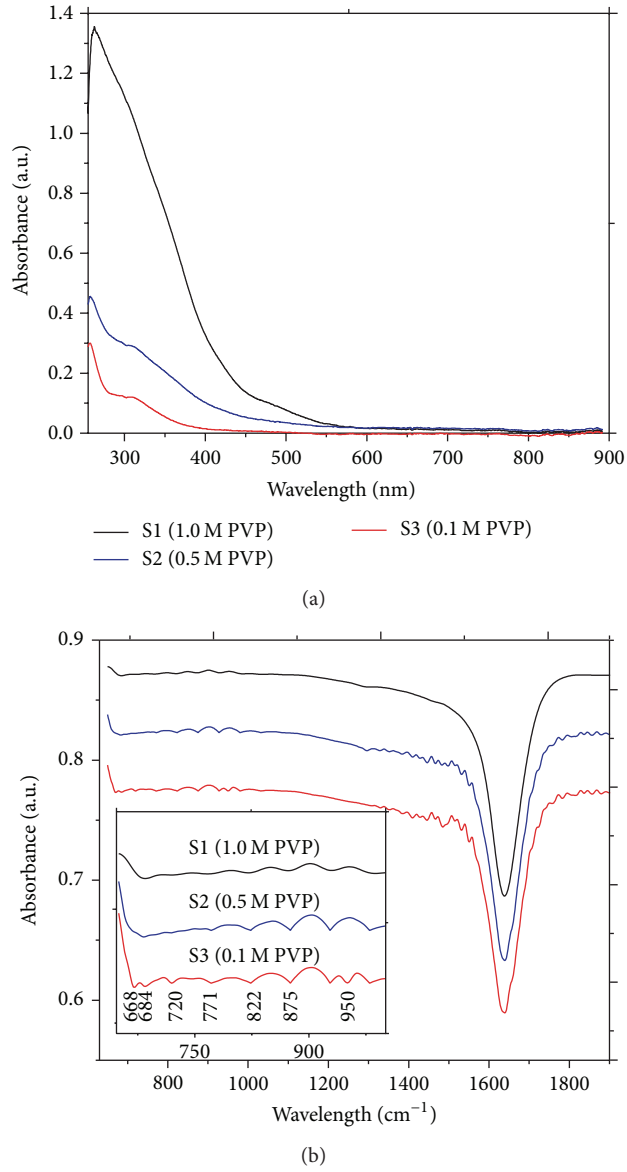

FIGURE 6: (a) UV-Vis and (b) IR analysis corresponding to nanoparticles synthesized with different concentrations of polyvinylpyrrolidone: 1.0 M (Fe), 0.5 M (Fe_3O_4), and 0.01 M.

IR spectrum of the sample S3, this intensity is dissociated into two bands situated at 771 and 822 cm^{-1} [27]. This band splitting can be explained by the effect of finite size of Fe_2O_3 nanoparticles, which generate several breaks in the atomic bonds of maghemite surface, producing an electrons rearrangement on the particle surface, and consequently a split of the energy levels of the maghemite [28]. On the other hand, a less-ordered maghemite (Fe_2O_3) structure can be identified by multiple lattice absorption bands within 800 cm^{-1} [26]. In the IR spectrum corresponding to the S3 sample, this behavior can be observed. Generally, maghemite structures partially ordered are associated with the cubic system, due to the vacancies in the maghemite structure [27, 28]. In this sense, the maghemite and magnetite show a spinel-like FCC structure with a network of oxygen that presents tetrahedral and octahedral coordination. However, distinctive element of maghemite is the presence of iron vacancies in the sublattice; the maghemite structure presents a vacancy of 2.67 cationic iron atoms located in octahedral sites [29]. The cation or vacancy distribution in octahedral positions can give rise to several crystal symmetries in maghemite which were identified in the XRD patterns. The magnetite oxidation to maghemite is described by the following equation [29]:

$$\left(Fe_8^{3+}\right)_t \left(Fe_8^{2+} Fe_8^{+3}\right)_o O_{32} \longrightarrow \left(Fe_8^{3+}\right)_t \left(Fe_{5.33\square 2.67}^{2+} Fe_8^{+3}\right)_o O_{32} \quad (2)$$

$$\text{Magnetite } Fe_3O_4 \longrightarrow \text{Maghemite } Fe_2O_3$$

where t represents the tetrahedral site, o is octahedral site, and $\square$ is vacancy.

The IR spectroscopy analysis confirms the oxidation carried out on the surface of the particles synthesized with lower amounts of stabilizer PVP. Consequently, it is clear that the surfactant acts on the surface of the particles, covering them and preventing the oxidization due to contact with the environment. It prevents agglomeration and growth of the particles as well.

4. Conclusions

Fe, Fe_3O_4, and Fe_2O_3 nanostructures were synthesized by a chemical reduction method. Fe nanoparticles are highly reactive due to the large presented surface area. According to the obtained results, the amount of surfactant agent provides an alternative for controlling the oxidation of the nanoparticles. A greater amount of surfactant agent provides more stability and homogeneous particles size as in the case of Fe_3O_4 particles. Different degrees of oxidation were observed as a function of the amount of stabilizing agent used during

the synthesis process. Evidently, this fact is attributed to a greater interaction between the nanostructures and the environment. The growth of branched nanostructures is due to the oxidation carried out first on the corners and edges of iron crystals because these sites show the greatest reactivity. The isotropic growth of these structures is performed on the entire surface of the crystal, in this case by the interaction of oxygen from the environment. This fact was proved by the oxidative etching process. As a result, in this novel synthesis route, the pH solution is constant and only the amount of PVP used in the synthesis process is the variable that determines the formation of Fe nanostructures.

Conflict of Interests

The authors declare that there is no conflict of interests regarding the publication of this paper.

References

[1] M. Abbas, B. P. Rao, S. M. Naga, M. Takahashi, and C. Kim, "Synthesis of high magnetization hydrophilic magnetite (Fe_3O_4) nanoparticles in single reaction—surfactantless polyol process," *Ceramics International*, vol. 39, no. 7, pp. 7605–7611, 2013.

[2] L. Shen, Y. Qiao, Y. Guo et al., "Facile co-precipitation synthesis of shape-controlled magnetite nanoparticles," *Ceramics International*, vol. 40, no. 1, pp. 1519–1524, 2014.

[3] K. Iwahori, J.-I. Watanabe, Y. Tani, H. Seyama, and N. Miyata, "Removal of heavy metal cations by biogenic magnetite nanoparticles produced in Fe(III)-reducing microbial enrichment cultures," *Journal of Bioscience and Bioengineering*, vol. 117, no. 3, pp. 333–335, 2014.

[4] R. Krzyminiewski, T. Kubiak, B. Dobosz, G. Schroeder, and J. Kurczewska, "EPR spectroscopy and imaging of TEMPO-labeled magnetite nanoparticles," *Current Applied Physics*, vol. 14, no. 5, pp. 798–804, 2014.

[5] J. Xu, H. Yang, W. Fu et al., "Preparation and magnetic properties of magnetite nanoparticles by sol–gel method," *Journal of Magnetism and Magnetic Materials*, vol. 309, no. 2, pp. 307–311, 2007.

[6] R. Long, S. Zhou, B. J. Wiley, and Y. Xiong, "Oxidative etching for controlled synthesis of metal nanocrystals: atomic addition and subtraction," *Chemical Society Reviews*, vol. 43, no. 17, pp. 6288–6310, 2014.

[7] Y. Wei, B. Han, X. Hu, Y. Lin, X. Wang, and X. Deng, "Synthesis of Fe_3O_4 nanoparticles and their magnetic properties," *Procedia Engineering*, vol. 27, pp. 632–637, 2012.

[8] Y.-F. Lin, J.-L. Chen, C.-Y. Xu, and T.-W. Chung, "One-pot synthesis of paramagnetic iron(III) hydroxide nanoplates and ferrimagnetic magnetite nanoparticles for the removal of arsenic ions," *Chemical Engineering Journal*, vol. 250, pp. 409–415, 2014.

[9] B. Andrzejewski, W. Bednarski, M. Kaźmierczak et al., "Magnetization enhancement in magnetite nanoparticles capped with alginic acid," *Composites Part B: Engineering*, vol. 64, pp. 147–154, 2014.

[10] K. Maaz, S. Karim, A. Mumtaz, S. K. Hasanain, J. Liu, and J. L. Duan, "Synthesis and magnetic characterization of nickel ferrite nanoparticles prepared by co-precipitation route," *Journal of Magnetism and Magnetic Materials*, vol. 321, no. 12, pp. 1838–1842, 2009.

[11] C. Meiorin, D. Muraca, K. R. Pirota, M. I. Aranguren, and M. A. Mosiewicki, "Nanocomposites with superparamagnetic behavior based on a vegetable oil and magnetite nanoparticles," *European Polymer Journal*, vol. 53, no. 1, pp. 90–99, 2014.

[12] L. Huang, F. Luo, Z. Chen, M. Megharaj, and R. Naidu, "Green synthesized conditions impacting on the reactivity of Fe NPs for the degradation of malachite green," *Spectrochimica Acta—Part A: Molecular and Biomolecular Spectroscopy*, vol. 137, pp. 154–159, 2015.

[13] G. Yang, B. Zhang, J. Wang, S. Xie, and X. Li, "Preparation of polylysine-modified superparamagnetic iron oxide nanoparticles," *Journal of Magnetism and Magnetic Materials*, vol. 374, pp. 205–208, 2015.

[14] P. I. P. Soares, A. M. R. Alves, L. C. J. Pereira et al., "Effects of surfactants on the magnetic properties of iron oxide colloids," *Journal of Colloid and Interface Science*, vol. 419, pp. 46–51, 2014.

[15] H.-L. Lien, D. W. Elliott, Y.-P. Sun, and W.-X. Zhang, "Recent progress in zero-valent iron nanoparticles for groundwater remediation," *Journal of Environmental Engineering and Management*, vol. 16, no. 6, pp. 371–380, 2006.

[16] D. Chen, S. Xiong, S. Ran, B. Liu, L. Wang, and G. Shen, "One-dimensional iron oxides nanostructures," *Science China: Physics, Mechanics and Astronomy*, vol. 54, no. 7, pp. 1190–1199, 2011.

[17] R. Frison, G. Cernuto, A. Cervellino et al., "Magnetite-maghemite nanoparticles in the 5–15 nm range: correlating the core-shell composition and the surface structure to the magnetic properties. A total scattering study," *Chemistry of Materials*, vol. 25, no. 23, pp. 4820–4827, 2013.

[18] X. Gou, G. Wang, X. Kong et al., "Flutelike porous hematite nanorods and branched nanostructures: synthesis, characterisation and application for gas-sensing," *Chemistry—A European Journal*, vol. 14, no. 19, pp. 5996–6002, 2008.

[19] J. Konopka, "Quantitative differentiation of three iron oxides by EDS," *Microscopy and Microanalysis*, vol. 19, supplement 2, pp. 1046–1047, 2013.

[20] E. Darezereshki, M. Ranjbar, and F. Bakhtiari, "One-step synthesis of maghemite (γ-Fe_2O_3) nano-particles by wet chemical method," *Journal of Alloys and Compounds*, vol. 502, no. 1, pp. 257–260, 2010.

[21] W. Kim, C.-Y. Suh, S.-W. Cho et al., "A new method for the identification and quantification of magnetite-maghemite mixture using conventional X-ray diffraction technique," *Talanta*, vol. 94, pp. 348–352, 2012.

[22] M. Girod, S. Vogel, W. Szczerba, and A. F. Thünemann, "How temperature determines formation of maghemite nanoparticles," *Journal of Magnetism and Magnetic Materials*, vol. 380, pp. 163–167, 2015.

[23] N. M. A. Hadia, S. García-Granda, J. R. García, D. Martínez-Blanco, and S. H. Mohamed, "Morphological and magnetic properties of the hydrothermally prepared α-Fe_2O_3 nanorods," *Materials Chemistry and Physics*, vol. 147, no. 3, pp. 1037–1041, 2014.

[24] C. Li, Y. Wei, A. Liivat, Y. Zhu, and J. Zhu, "Microwave-solvothermal synthesis of Fe_3O_4 magnetic nanoparticles," *Materials Letters*, vol. 107, pp. 23–26, 2013.

[25] M. Stoia, C. Păcurariu, R. Istratie, and D. Nižňanský, "Solvothermal synthesis of magnetic Fe_xO_y/C nanocomposites used as adsorbents for the removal of methylene blue from wastewater," *Journal of Thermal Analysis and Calorimetry*, 2015.

[26] S. Chandrasekaran, S. H. Hur, E. J. Kim et al., "Highly-ordered maghemite/reduced graphene oxide nanocomposites for high-performance photoelectrochemical water splitting," *RSC Advances*, vol. 5, no. 37, pp. 29159–29166, 2015.

[27] S. Babay, T. Mhiri, and M. Toumi, "Synthesis, structural and spectroscopic characterizations of maghemite γ-Fe_2O_3 prepared by one-step coprecipitation route," *Journal of Molecular Structure*, vol. 1085, pp. 286–293, 2015.

[28] P. Synek, O. Jašek, and L. Zajíčková, "Study of microwave torch plasmachemical synthesis of iron oxide nanoparticles focused on the analysis of phase composition," *Plasma Chemistry and Plasma Processing*, vol. 34, no. 2, pp. 327–341, 2014.

[29] W. S. Peternele, V. Monge Fuentes, M. L. Fascineli et al., "Experimental investigation of the coprecipitation method: an approach to obtain magnetite and maghemite nanoparticles with improved properties," *Journal of Nanomaterials*, vol. 2014, Article ID 682985, 10 pages, 2014.